Vibronic assignments and vibronic coupling in the $^1E''$ state of sym-triazine by two photon spectroscopy

J. D. Webb, K. M. Swift, and E. R. Bernstein

Citation: The Journal of Chemical Physics **73**, 4891 (1980); doi: 10.1063/1.440018
View online: http://dx.doi.org/10.1063/1.440018
View Table of Contents: http://aip.scitation.org/toc/jcp/73/10
Published by the American Institute of Physics

Vibronic assignments and vibronic coupling in the $^1E''$ state of *sym*-triazine by two photon spectroscopy[a)]

J. D. Webb,[b)] K. M. Swift, and E. R. Bernstein

Department of Chemistry, Colorado State University, Fort Collins, Colorado 80523
(Received 2 July 1980; accepted 31 July 1980)

Two photon photoacoustically detected spectra are reported for the first excited singlet state $^1E''$ of *sym*-triazine in the gas phase. The origin has been positively identified as of E'' symmetry through contour calculations and hot band observations. The excited state absorption is dominated by a highly irregular ν_6' progression. These observations include: $6_0^1(A_1'') \sim 0\ cm^{-1}$, $6_0^1(E'') \sim 227\ cm^{-1}$, $6_0^2(E'') \sim 556\ cm^{-1}$, $6_0^3(E'') \sim 693\ cm^{-1}$, and possibly $6_0^4(E'')$ [$8_0^1(E'')$ or $19_0^1(E'')$] $\sim 836\ cm^{-1}$ above the $^1E''$, origin. The one photon observed $6_0^1(A_2'')$ and $6_0^2(A_2'')$ bands at 677 and 1176 cm^{-1} respectively, fit in well with these assignments. These observations are strongly supported by a Jahn–Teller calculation which predicts: little coupling betwwen the A_2'' and E'' electronic manifolds; a large quadratic coupling and a small linear coupling in the E'' manifold; and a quenched angular momentum in this state. Good agreement is shown to exist between one photon and two photon spectroscopic observations and the calculations.

I. INTRODUCTION

The molecular properties of *sym*-triazine ($C_3N_3H_3$) have been of considerable continued interest over the past 25 years.[1–16] Optical spectroscopy has been one of the major ongoing efforts in the study of geometry, excited state energy levels, and dynamics of *sym*-triazine. There are a number of reasons for this. First, *sym*-triazine is of high molecular symmetry (D_{3h}) with relatively few atoms, thereby reducing its vibrational and electronic complexity to some extent. Second, it is the only small aromatic molecular system with a degenerate, readily accessible, first excited state. Third, vibronic coupling in this system can be quite extensive; both intrastate [Jahn–Teller (JT)] and interstate [pseudo-Jahn–Teller (PJT)] couplings are potentially large. Fourth, the molecule is of considerable biological interest, particularly as a model system for many other nitrogen heterocycles. Fifth, radiationless relaxation from the lowest singlet and triplet states is fast and for the most part poorly understood. In view of the foregoing, it was thought that the new technique of two photon spectroscopy would be an excellent method for the further study of this system.

The first optical spectrum of triazine vapor located a broad, intense transition at 272 nm,[1] which was assigned by solvent shift studies as $n \rightarrow \pi^*$ (A_2'').[2,4] Subsequent analysis of the hot band region showed many of the weak, sharp features were associated with an electric dipole (one photon) forbidden E'' state.[8] Low temperature crystal studies have confirmed these assignments.[9–13] Single vibronic level fluorescence (SVLF) spectra are also in agreement with this conclusion.[14]

The $^1E'' \leftarrow {}^1A_1'$ transition is two photon allowed and it was felt two photon spectroscopic experiments would be an obvious way to increase our understanding of the excited state, its geometry, vibronic coupling, and relaxation processes. However, since triazine is known to emit only weakly, two photon excitation experiments employing conventional detection techniques (fluorescence) were not expected to be successful. Photoacoustic detection does, however, provide a straightforward, reliable method for obtaining the desired gas phase spectra. We have recently reported preliminary results of two photon experiments on triazine detected by means of the photoacoustic effect and by fluorescence from photochemically generated cyanyl (CN).[17] This paper presents more complete results and a more detailed discussion of our findings and conclusions. (It should be noted that some of the previous assignments have been changed in the present paper due to new experimental and theoretical findings but that the general conclusions remain unaltered.)

Vibronic assignments are made with the help of rotational contour analysis and polarization studies.[18,19] The isotropic part of the Q branch of a totally symmetric vibronic state will be observed in absorption if viewed in linearly polarized light but will not be observed if circularly polarized light is employed. The polarization behavior of hot bands can be used to imply the vibronic symmetry of the corresponding cold bands (Sec. IV). With these methods, combined with other standard techniques of spectroscopic analysis, it has been possible to give a unique assignment for most of the major features of the $^1E'' \leftarrow {}^1A_1'$ absorption spectrum.

The presentation is organized as follows: In Sec. II we present background information on triazine and Jahn–Teller (JT) coupling. Section III describes experimental details of the two photon photoacoustic and fluorescence apparatus employed. In Sec. IV we present experimental results. Rotational contour and vibronic coupling calculations used to understand the spectroscopic assignments are given in Sec. V. Manifestations of the JT effect in the $^1E''$ state are discussed in Sec. VI. Our findings are summarized in Sec. VII.

II. BACKGROUND

Early spectroscopic studies of *sym*-triazine[1,2,4] suggested the energy level diagram and excited state symmetries shown in Fig. 1. The intense portion of the 272

[a)]Supported in part by the Office of Naval Research.
[b)]Present address: Shell Development Company, Westhollow Research Center, P. O. Box 1380, Houston, TX 77001.

 0021-9606/80/224891-13$01.00

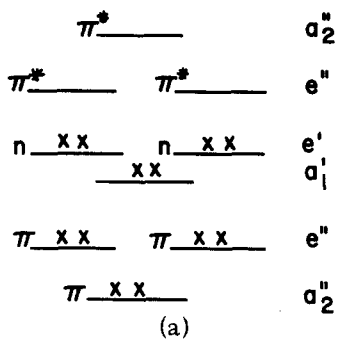

ELECTRON PROMOTION	STATE SYMMETRY	TRANSITION TYPE
$\pi^*(e'') \leftarrow n(e')$	E''	2 PHOTON
	A_2''	1 PHOTON
	A_1''	
$\pi^*(e'') \leftarrow n(a_1')$	E''	2 PHOTON

(b)

FIG. 1. (a) Ground state n, π electronic structure. (b) $\pi^* \leftarrow n$ spectroscopic transitions.

nm band observed in one photon spectra is seen to be the one photon allowed A_2'' electronic state. However, Brinen's identification of the electronic origin was subsequently shown to be incorrect.[4,8] Ground state vibrational frequencies and rotational constants were determined by infrared and Raman spectroscopy[3,5]; these are given in Table I. Ground state geometry was determined to be planar, and of D_{3h} symmetry.

Udagawa's partial rotational contour analysis of one of the weak, sharp bands on the low energy side of the 272 nm band indicated that triazine is planar (or at least nearly so) in its lowest excited singlet state.[7] Fisher and Small were able to assign some of the sharp, weak transitions on the low energy side of the 272 nm band as being due to an E'' electronic state by consideration of vibronic selection rules and by identification of some vibronically allowed hot bands.[8] They realized that JT coupling within the E'' manifold was possible but they were unable to find definitive evidence for it. A summary of their vibrational assignments is given in Table II.

TABLE I. Ground state vibrations of *sym*-triazine.

Symmetry type	Predominant motion of mode	Lord numbering[a]	Frequency (cm^{-1})[b] h_3	d_3
	Hydrogen stretch	2	3042	2293
a_1'	In-plane ring bend	12	1132	1077
	Ring stretch	1	992	987
a_2'	Ring stretch	14	1617	1586
	In-plane hydrogen bend	3 or 15	1251	951
	In-plane hydrogen bend	20	3056	2280
	Ring stretch	8	1556	1530
e'	Ring stretch	19	1410	1284
	In-plane hydrogen bend	9	1174	931
	In-plane ring bend	6	675	662
a_2''	Out-of-plane ring bend	5	925	861
	Out-of-plane ring bend	4	737	577
e''	Out-of-plane hydrogen bend	10	1031	846
	Out-of-plane ring bend	16	340	309

Ground state rotational constants (cm^{-1})[c]

$h_3 = 0.2146 \quad d_3 = 0.19358$

[a] R. C. Lord, A. L. Marston, and F. A. Miller, Spectrochim. Acta 9, 113 (1957).
[b] Reference 5.
[c] J. E. Lancaster and B. P. Stoicheff, Can. J. Phys. 34, 1016 (1956).

Knight and Parmenter's SVLF data[14] on *sym*-triazine support these E'' electronic and $6_0^1(A_2'')$ vibronic assignments. Only ν_6 appears to be active in the SLVF spectra, indicating that a model in which a single vibrational mode vibronically couples to the E'' electronic state is reasonable. This situation is to be contrasted to that found for benzene[20] and transition metal hexafluorides.[21-23] Furthermore, the SVLF intensity pattern for the ν_6 progression $[I(6_2^1) > I(6_4^1) \gg I(6_3^1) \sim I(6_5^1) \sim I(6_6^1)]$ indicates that quadratic JT (QJT) coupling is more important than linear JT (LJT) coupling. If LJT vibronic coupling is dominant, the pumped level [the $n=1$ $\nu_6(A_2'')$ vibronic component in the $^1E''$ excited state] will be mixed with all other $\nu_6(A_2'')$ components $(n \geq 2)$ in the $^1E''$ electronic state, since LJT coupling has the selection rule $\Delta n = \pm 1$. In order for emission to occur, the electric dipole allowed $^1A_2''$ electronic state about 1500 cm^{-1} above the $^1E''$ origin must be mixed into the pumped level as well. LPJT coupling will mix $\nu_6(A_2'')$ components $(n = 0, 2, 3, \ldots)$ of the $^1A_2''$ electronic state into the pumped level with the selection rule $\Delta n = \pm 1$. Since the pumped level has contained in it all $\nu_6(A_2'')$ levels of the $^1E''$ electronic state (due to LJT coupling), LPJT coupling will mix in all $\nu_6(A_2'')$ components of the $^1A_2''$ electronic state to some extent. Note that this coupling omits ν_6 $n=1$ of $^1A_2''$ which is of E'' vibronic symmetry. QJT coupling,

TABLE II. Electronic origins and vibrational analysis of the $^1E''$ state determined from one photon spectra.

Electronic origin (cm^{-1})[a]		Rotational constant B' (cm^{-1})[b]	
h_3	30 870	0.212	
d_3	30 989	0.191	

Vibration	h_3[a]	d_3[a]	h_3[b]	d_3[b]
6	677(∥)	664(∥)	677	664
e' 2×6	···	···	1176	1145
8	1176(∥)	1145(∥)	1005	960
19	···	···	1105	1048
a_2'' 4	359(⊥)	278(⊥)	359	278
5	599(?)	559(⊥)	599	559
e'' 10	508(⊥)	417(⊥)	508	417
16	303(⊥)	273	308	280
a_1' 12	1081	1035	1081	1035

[a] Reference 8. [b] Reference 24.

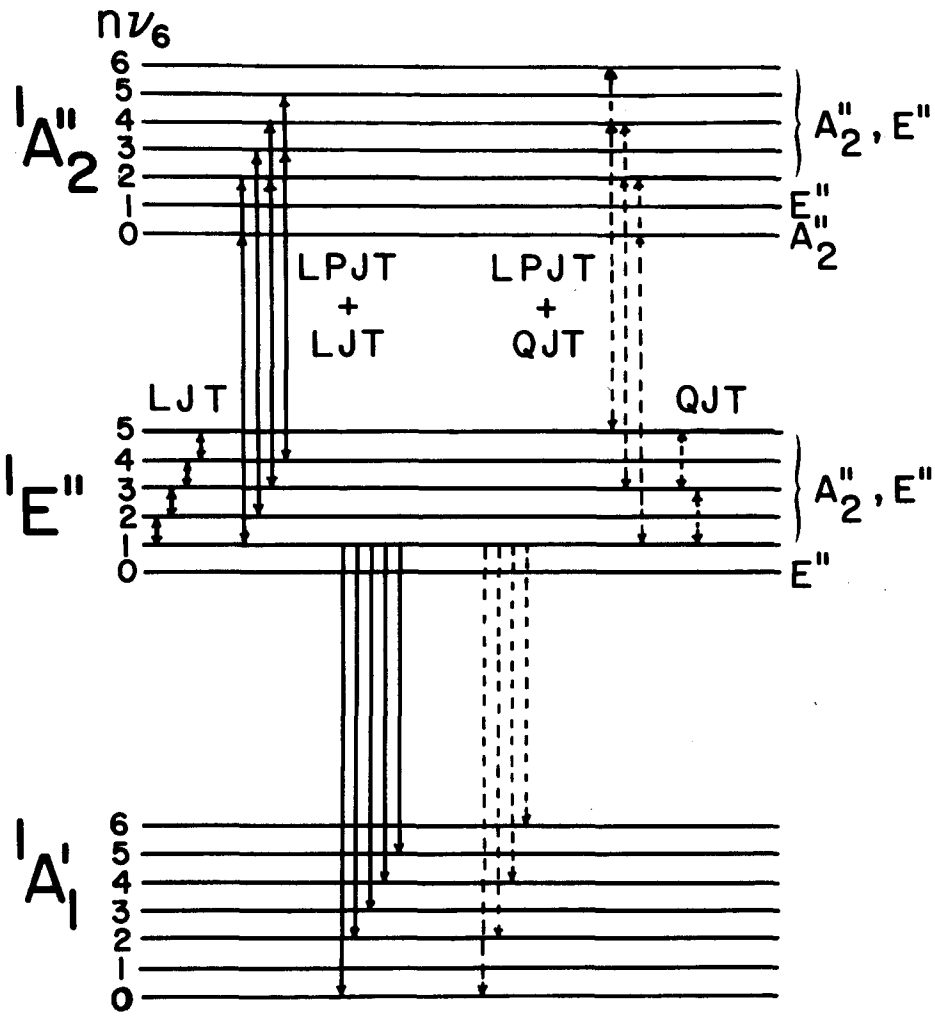

FIG. 2. Role of vibronic coupling in single vibronic level fluorescence (SVLF). See the text (Sec. II) for detailed discussion. The left hand side of the figure shows the electronic symmetry and the numbers indicate the number of quanta of ν_6. The right hand side shows the relevant vibronic symmetries of the levels. Double-ended arrows show vibronic coupling pathways. Single-ended arrows going down indicate possible emission. Solid lines are the LJT coupling case, and dashed lines are the QJT coupling case.

on the other hand, will mix ν_6 components of the $^1E''$ electronic state according to the selection rule $\Delta n = 0, \pm 2$. Thus, the $n=1$ $\nu_6(A_2'')$ level which is being pumped will contain the other $\nu_6(A_2'')$ components of the $^1E''$ electronic state with *odd n*. LPJT coupling will mix in *even* $\nu_6(A_2'')$ components from the $^1A_2''$ electronic state according to the LPJT selection rule $\Delta n = \pm 1$. The intensity of the emission progression $6_n^1(A_2'')$ ($^1E'' - {}^1A_1'$) will be proportional to $\langle {}^1A_2'' n' | r | {}^1A_1' n \rangle = \langle {}^1A_2'' | r | {}^1A_1' \rangle \langle n' | n \rangle$, which, in the absence of large Franck–Condon shifts, will be greatest for $n' = n$. With LJT coupling mixing $n = 0, 2, 3, 4, \ldots$ $\nu_6(A_2'')$ levels of the $^1A_2''$ electronic state into the pumped level, emission should occur to ν_6 levels $n = 0, 2, 3, 4, \ldots$ of the ground state. With QJT coupling dominant, the pumped level contains only *even n* $\nu_6(A_2'')$ components from the $^1A_2''$ electronic state, so emission will occur to even n ν_6 levels in the ground electronic state, thus predicting $I(6_3^1) \sim 0$ and $I(6_4^1)$ large, in agreement with the experimental SVLF data. Figure 2 illustrates this effect and how it comes about.

Barnard has carried out high resolution one photon studies of *sym*-triazine vapor and has done a careful rotational contour analysis.[24] He concluded that electronic angular momentum in the $^1E''$ state is largely quenched ($-0.2 < \zeta_e < 0.1$). A summary of his other results is included in Table II. An important conclusion from this work is that the 6_0^2 (A_2'') state is only 499 cm^{-1} above the 6_0^1 (A_2'') at 677 cm^{-1}. Such an energy level pattern is predicted by QJT calculations but never by LJT calculations.

The above discussion intimates that the QJT vibronic coupling is important in the E'' electronic state of *sym*-triazine. Previous theoretical investigations of a QJT coupling have shown that it can be more influential in a given circumstance than might be obvious intuitively.[21–23] Some vibronic levels are effected by QJT coupling in first order perturbation theory whereas LJT coupling effects vibronic levels only in second order perturbation theory. A large quadratic JT effect is present in ReF_6[21] and IrF_6.[22] In addition, calculations for these molecules which allowed simultaneous JT coupling in two modes led to quite different results than if the two modes were considered separately.

III. EXPERIMENTAL

Synthesis of h_3- and d_3-*sym*-triazine samples used in this study is described in Refs. 13 and 25. Additional purification steps such as vacuum distillation, fusion with potassium, and distillation through a molecular sieve were carried out in a grease-free vacuum system.

Initial two photon photoacoustic experiments were per-

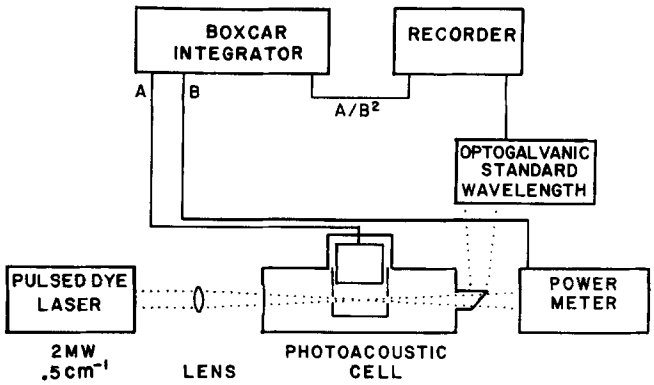

FIG. 3. Experimental two photon photoacoustic apparatus (see the text for discussion).

formed in a sample cell with windows sealed with lightly greased O rings. It was found that HCN appeared as a decomposition product in such a cell. HCN evolution was monitored photoacoustically (one photon absorption) by observing the fifth overtone of the carbon–hydrogen stretch ($\nu_3 = 3312$ cm^{-1} and $5\nu_3 = 15\,552$ cm^{-1}) which appears fortuitously in the midst of the two photon triazine spectrum. Subsequently, all two photon gas phase cells had windows sealed with indium gaskets; to the limit of our detection ability no HCN is produced in these new cells. However, decomposition is a problem in these experiments nonetheless, as triazine is apparently photodecomposed by an n photon process that is, in any event, two photon resonant. This photochemical process yields CN radicals. CN is detected photoelectrically by monitoring $B \rightarrow X$ emission in the near ultraviolet, as cyanyl is produced in its excited state. CN is also observed in two photon absorption $B \leftarrow X$ followed by emission. The overall process for this photochemistry is described as follows:

$$C_3N_3H_3 \xrightarrow{nh\nu} CN^* + \text{other products} \rightarrow CN + h\nu' \ ,$$

$$CN + 2h\nu'' \rightarrow CN^* \rightarrow CN + h\nu' \ .$$

CN two photon absorption is not observed photoacoustically, due either to high quantum yield for emission or low concentration of total photoproducts. CN production involves a two photon resonant triazine process and, with the exception of the readily identified CN absorption $[B(v=3) \leftarrow X]$, CN fluorescence gives the same triazine line shapes and positions as does the photoacoustically detected spectrum. Some variations in relative intensities of vibronic features have been previously noted,[17] however.

All features observed in the two photon photoacoustically detected spectrum are due only to *sym*-triazine. This is confirmed by the existence of hot bands separated from cold bands by triazine ground state frequencies. Also, the d_3-triazine origin is blue shifted by over 100 cm^{-1} while most of the vibrational intervals are almost unchanged.

The experimental arrangement of the two photon photoacoustic apparatus is depicted in Fig. 3. The tunable laser for these experiments is a Nd/YAG pumped dye laser (Quanta-Ray DCR-1 and PDL) with an output of 2 MW over the range 6200–6600 Å using DCM dye. The laser beam is focused in front of a 1 in. condenser microphone (B & K 4145) mounted in a high vacuum stainless steel cell. A unique feature of this cell design is that a Teflon cup has been mounted on the microphone body in order to enhance signals and reduce background; the best signal occurs for the situation in which the distance between the microphone diaphragm and the end plate of the cup is as small as possible. Apparently, two factors are important: focus should be as close to the disphragm as possible, and the shock wave reflected from the cup should reach the diaphragm while it is still deformed from the initial shock wave. This latter situation insures better signal integration.[26]

Other important cell design features are absence of grease or epoxy; metal (Cu) flange seals and indium window seals; metal–ceramic feedthrough for microphone electrical connections; and Brewster output window of glass-blown quartz and molybdenum sealed. The angled output window eliminates background signals from reflected laser light impinging on the microphone assembly. An angled input window is less necessary and makes polarization experiments difficult.

The microphone signal is amplified (PAR 114/118 amplifier) and is processed by a boxcar integrator (PAR 164/162) (channel A). The laser power level is monitored by a pyroelectric power meter (Molectron) and processed in the second (B) channel of the boxcar. The two signals are subsequently ratioed (A/B^2) to compensate for pulse-to-pulse variations and the power curve of the dye laser. Wavelength calibration is achieved by splitting off a small fraction of the dye laser beam and using the optogalvanic effect in a standard Fe–Ne hollow cathode lamp to observe well known atomic resonances. Circularly polarized light was produced in a Fresnel rhomb. Hot band experiments were performed at 100 °C by heating the cell with a heating tape. The signal to noise ratio for these experiments was about a factor of 2 to 3 lower than for room temperature experiments due to depleted ground state population, convection currents in the cell, and increased microphone noise.

Two photon emission excitation experiments were also attempted (both fluorescence and phosphorescence). The experimental arrangement is similar to the above except a photomultiplier tube (RCA 8850) with appropriate filters was used as a detector. Pulses from the 8850 were fed into the boxcar integrator directly. At 10 Torr of *sym*-triazine vapor, no triazine emission was detected. However, emission from CN was observed, as previously described, and since it is two photon triazine resonant, the absorption could be followed with the $B \rightarrow X$ CN emission. Even at 0.1 Torr only weak CN emission could be detected from the sample.

IV. EXPERIMENTAL RESULTS

Two photon photoacoustic spectroscopic data for h_3- and d_3-triazine are found in Table III and representative survey spectra and individual band contours can be found

TABLE III. Summary of observed two photon spectra of *sym*-triazine (h_3) and (d_3).

λ_{vac} (Å) h_3		$2\sigma_{vac}$ (cm^{-1}) h_3	$\Delta 2\sigma_{vac}$ (cm^{-1}) h_3	d_3	I[a]	Assignments[b]
6634.0		30 148	−729	−704	W	6_1^1 (A_1'')
6630.9		30 162	−715	−692	W	
6628.2		30 174	−703	−680	W	6_1^0; 16_2^0
6624.5		30 191	−686	−664	W	
6578.7		30 401	−476	−465	W	6_1^1 (E'')
6550.8		30 531	−346	−313	W	16_1^0[c]
6528.3		30 636	−241		W	$6_1^0\,16_0^1$ (A_1'); $16_2^0\,16_0^1$ (A_1')
6506.2		30 740	−137	−115	W	$16_1^0\,6_0^1$ (E'')[c]
6502.6		30 757	−120		W	6_1^2 (E''); $16_2^0\,6_0^2$ (E'')
6482.4		30 852	−24	−28	W	6_0^1 (A_1'') (?); 16_1^1 (E')
6480.7		30 861	−16	−16	S	Origin of E'' electronic state (30 869 cm^{-1})
6477.3	h_3	30 877[d]	0		S	
	d_3	30 995		0		
6474.3		30 891	14	10	M	
6459.0		30 965	88	96	W	16_1^1 (A_1')
6455.3		30 982	105	111	W	
6454.2		30 988	111		W	
6436.2		31 074	198	185	M	6_0^1 (E'') (31 096 cm^{-1})
6433.6		31 087	210	201	S	
6432.6		31 091	215	206	M	
6430.4		31 102	225	218	M	
6414.3		31 180	303	297 314[e]	M	$16_1^1\,6_0^1$ (A_1')
6387.1		31 313	436	413	M	16_0^1 (A_1')[c]
6385.3		31 322	445		M	10_0^1 (A_1')[c] (?)
6375.1		31 372	495	476	W	$16_1^0\,6_0^4$ (E'') [$16_1^0\,8_0^1$ (E'') or $16_1^0\,19_0^1$ (E'')][c]
6366.1		31 416	539	535	S	6_0^2 (E'') (31 425 cm^{-1})
6362.8		31 433	556	548	VS	
6360.0		31 446	570	562	M	
6343.7		31 527	650		W	$16_1^1\,6_0^2$ (A_1')
6340.7		31 542	665		W	
6338.2		31 555	678	665	M	6_0^3 (E'') (31 562 cm^{-1})
6335.0		31 570	693	675	M	
				680[e]		
6332.1		31 585	708	692	M	
6328.5		31 603	726		W	
6309.0		31 701	824	771	M	6_0^4 (E'') [8_0^1 (E'') or 19_0^1 (E'')] (31 705 cm^{-1})
6306.5		31 713	836	791	S	
6303.0		31 731	854	799	M	
				804[e]		
6288.9		31 802	925		W	
6270.4		31 896	1019		W	
6267.1		31 912	1036	996	VS	$12_0^1\,6_0^1$ (A_1')
6263.1		31 933	1056	1009	VS	12_0^1 (E'') (31 940 cm^{-1})
6260.3		31 948	1071	1020	VS	
6238.2		32 061	1184		S	
6227.5		32 116	1239		M	
6224.4		32 131	1254		M	
6218.8		32 160	1283	1224 1240[e]	M	$12_0^1\,6_0^1$ (E'')
6207.8		32 218	1340		S	

TABLE III (*Continued*)

λ_{vac} (Å) h_3	$2\sigma_{vac}$ (cm^{-1}) h_3	$\Delta 2\sigma_{vac}$ (cm^{-1}) h_3	d_3	I[a]	Assignments
6203.9	32 237	1360		S	
6199.3	32 261	1385		S	
6175.8	32 384	1507	1430	M	$12_0^1\,16_0^1$ (A_1')
6156.5	32 486	1609		S	
6153.3	32 503	1626	1568	VS	$12_0^1\,6_0^2$ (E'')
6149.8	32 521	1644		S	
6148.1	32 530	1653		S	
6141.4	32 566	1689		M	
6128.8	32 633	1756		S	
6120.7	32 676	1799		VS	
6101.1	32 781	1904		M	$12_0^1\,6_0^4$ (E'') [$12_0^1\,8_0^1$ (E'') or $12_0^1\,19_0^1$ (E'')]
6064.1	32 981	2104		VS	
6055.0	33 031	2154		M	
6051.5	33 050	2173		M	
6034.6	33 142	2265		M	
6030.3	33 166	2289		M	

[a] I = intensity; W = weak; M = moderate; S = strong; VS = very strong.
[b] See the text (Sec. IV) for explanations. Parenthetical symmetry is the excited state symmetry. Rotationless origins are given in parentheses (± 3 cm^{-1}) for h_3-*sym*-triazine.
[c] Feature shows the change in intensity with circularly polarized light.
[d] This strong, sharp feature is taken as the origin for purposes of measuring $\Delta 2\sigma_{vac}$ and approximate vibrational intervals.
[e] Features in d_3 are split.

in Figs. 4–9. The first step in assigning the spectrum is to determine the excited state vibronic symmetry for each of the bands. Rotational contour simulation can often associate a unique ΔK selection rule with a given contour, which immediately gives the vibronic symmetry (see Table IV).[27] This method gives the symmetry of the lowest energy cold band as E''. Such an assignment is supported by the presence of a polarized hot band at -346 cm^{-1}. This frequency is close to the ground state value for $\nu_{16}''(e'')$. The transition assignment $^1E'' \leftarrow {}^1E''$ ($e''\,{}^1A_1'$) (16_1^0) explains both the location and polarization behavior of the band (Table IV). The lowest cold band is thus identified as an E'' origin. The 556, 693, 836, and 1071 cm^{-1} features are assigned in a similar manner as E'' vibronic states. The 210 cm^{-1} band (see Fig. 8) does not have an easily recognizable E'' rotational

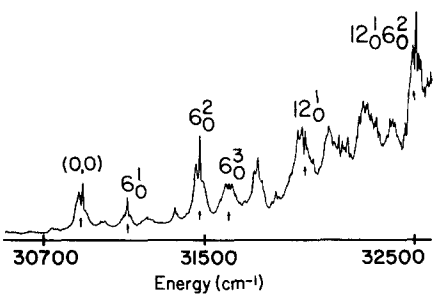

FIG. 4. Survey two photon photoacoustic spectrum of h_3-*sym*-triazine. Arrows indicate rotationless origins of labeled features. Horizontal axis is not linear in frequency, but in wavelength.

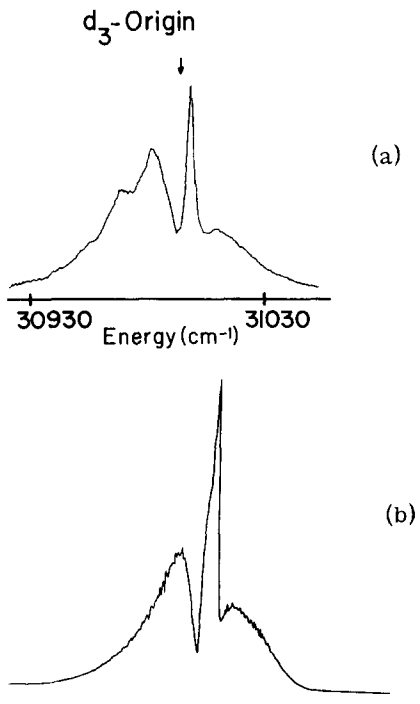

FIG. 5. (a) Experimental rotational contour for d_3-*sym*-triazine $^1E''$ origin. The rotationless origin is marked with an arrow. The shoulder at low energy side of contour could be related to the presence of 6_0^1 (A_1''). See the text (Sec. IV) for discussion. (b) Calculated rotational contour of origin with $\Delta K = \pm 1$, $B'' = 0.19358$ cm^{-1}, $B' = 0.1916$ cm^{-1}, $C'' = B''/2$, $C' = B'/2$, $\zeta = +0.1$, $T = 298$ K. The frequency scale is the same for the Fig. 5(a). Note the missing shoulder on the low energy side of the contour.

contour (*vide infra*), but it may be assigned as E'' with confidence, since its ν_{16}'' hot band is polarized and an E'' contour can be calculated for it. An A_1' band is observed at 436 cm^{-1} by its polarization behavior. No E' contours are identified.

It is somewhat more difficult to determine the vibrational parentage of each transition. The A_1' band at 436 cm^{-1} must be due to an e'' vibration, since only $e''\times E''$ contains A_1' in D_{3h}. It is thus either 16_0^1 (A_1') or 10_0^1 (A_1'). Since it has a small isotope shift 10_0^1 (A_1'), an out of plane hydrogen bending motion, can be ruled out. Also, the ν_{16}'' hot band of this transition is unusually intense, implying that it is a sequence band (16_1^1). The weaker polarized feature at 445 cm^{-1} in h_3 spectra is not a hot band and is tentatively assigned as 10_0^1 (A_2'). Since it does not evidence a 10_1^1 sequence band ~ -585 cm^{-1} and a comparable set of features is not located in d_3 spectra, this assignment remains less certain than 16_0^1 (A_1'). It should be noted that both these values (436 and 445 cm^{-1}) are quite different from those reported in Table II based on one photon results. However, both ν_{10} and ν_{16} are e'' modes with vibronic components A_1' (two photon allowed), A_2' (forbidden), and E' (one photon allowed); thus, the two experiments observe different vibronic components. In this work we have not analyzed the cause of this splitting

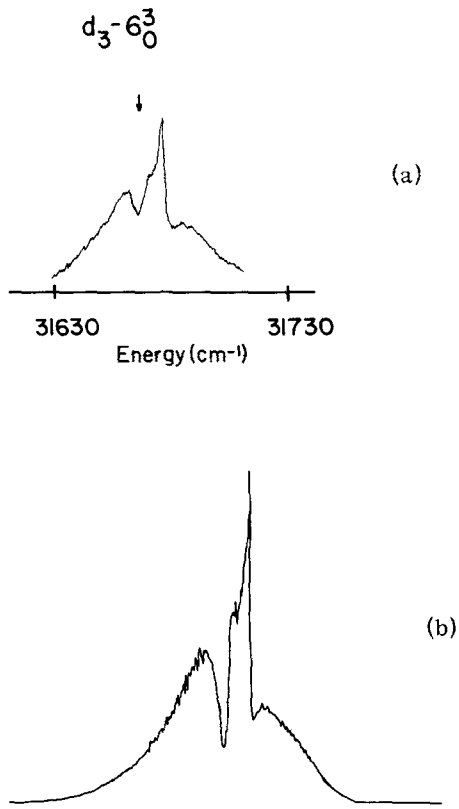

FIG. 7. (a) Experimental rotational contour for d_3-*sym*-triazine 6_0^3. The rotationless origin is marked with an arrow. (b) Calculated rotational contour of 6_0^3 with $\Delta K = \pm 1$, $B'' = 0.19358$ cm^{-1}, $B' = 0.1915$ cm^{-1}, $C'' = B''/2$, $C' = B'/2$, $\zeta = 0.0$, $T = 298$ K. The frequency scale is the same as for Fig. 7(a).

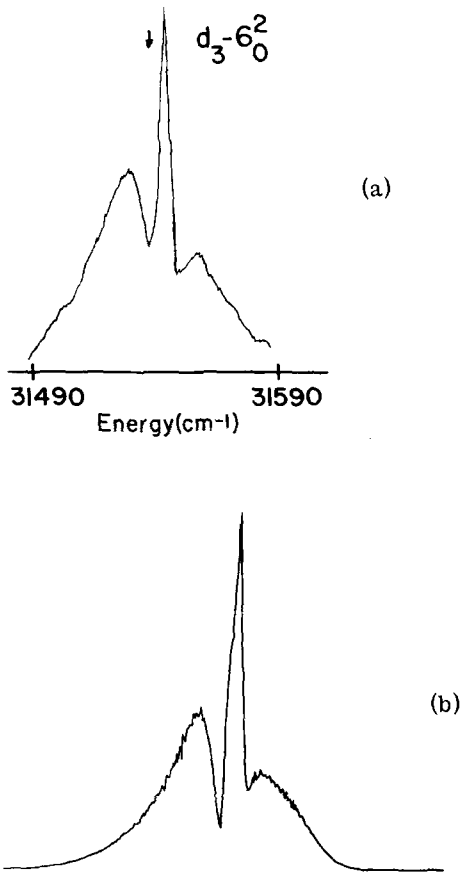

FIG. 6. (a) Experimental rotational contour for d_3-*sym*-triazine 6_0^2. The rotationless origin is marked with an arrow. (b) Calculated rotational contour of 6_0^2 with $\Delta K = \pm 1$, $B'' = 0.19358$ cm^{-1}, $B' = 0.1916$ cm^{-1}, $C'' = B''/2$, $C' = B'/2$, $\zeta = +0.1$, $T = 298$ K. The frequency scale is the same as for Fig. 6(a).

TABLE IV. Vibronic symmetries and selection rules in an E'' state.

D_{3h} vibrational symmetry	Vibronic symmetry of the first quantum in the E'' electronic state
a_1'	E''
a_2'	E''
e'	A_1', A_2', E''
a_2''	E'
e''	A_1', A_2', E'

Type	Vibronic symmetry	Selection rule
One-photon	A_2''	$\Delta K = 0(\parallel)$
	E'	$\Delta K = \pm 1(\perp)$
Two-photon	A_1'	$\Delta K = 0$[a]
	E''	$\Delta K = \pm 1$
	E'	$\Delta K = \pm 2$

[a] For $A_1' \leftarrow A_1'$ or $E'' \leftarrow E''$ the transition symmetry is A_1' ($\Delta K = 0$) and the isotropic part of the Q branch disappears if the transition is observed in circularly polarized light.

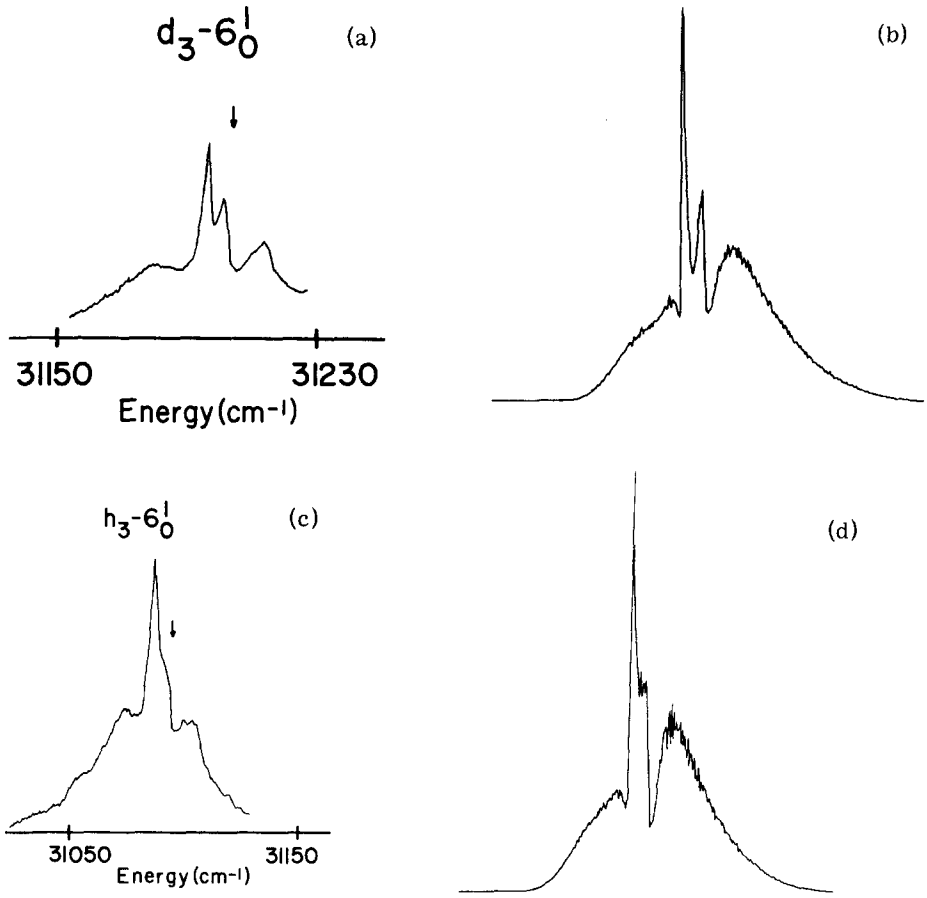

FIG. 8. (a) Experimental rotational contour for d_3-*sym*-triazine 6_0^1. The rotationless origin is marked with an arrow. (b) Calculated rotational contour of 6_0^1 with $\Delta K = \pm 1$, $B'' = 0.19358$ cm^{-1}, $B' = 0.1962$ cm^{-1}, $C'' = B''/2$, $C' = B'/2$, $\zeta = -0.1$, $T = 298$ K. The frequency scale is the same as for Fig. 8(a). (c) Experimental rotational contour for h_3-*sym*-triazine 6_0^1. The rotationless origin is marked with an arrow. (d) Calculated rotational contour with $\Delta K = \pm 1$, $B'' = 0.2146$ cm^{-1}, $B' = 0.2172$ cm^{-1}, $C'' = B''/2$, $C' = B'/2$, $\zeta = 0.0$, $T = 298$ K. The frequency scale is the same as for Fig. 8(c).

but it must arise from either anharmonicities leading to ν_{16}–ν_{10} coupling, quadratic intrastate vibronic coupling, or strong Herzberg–Teller coupling with E', A_1', or A_2' electronic states. It would certainly be interesting to pursue the causes of these vibronic splittings.

The totally symmetric vibration $12_0^1(E'')$ is identified by its known frequency,[8] its similarity in line shape and structure to the origin, and by the non-totally symmetric modes built on it. Most of the remaining bands in the region below $(0,0) + 1000$ cm^{-1} are of E'' vibronic symmetry and could be of a_1', a_2', or e' vibrational parentage. We rule out the a_1' totally symmetric vibrations since no Franck–Condon progressions are observed and non-totally symmetric vibrations are not built on any of these features. Since isotope shifts are small for these low lying modes ν_3', ν_{20}', and ν_9' may be eliminated as candidates. The ground state frequency of ν_{14} is too high and it can only appear via Herzberg–Teller coupling which would not be capable of producing the observed intensity. The only remaining vibrational assignments for the four E'' bands below $(0,0) + 1000$ cm^{-1} are ν_8', ν_{19}', and ν_6'. Since in the one photon vibronically allowed spectrum $6_0^1(A_2'')$ has been assigned at 677 cm^{-1}, we can assume that ν_6' is the lowest energy of the e' excited state modes; $8_0^1(A_2'')$ and $19_0^1(A_2'')$ appear to be over 1000 cm^{-1} (Table II) from the origin. Thus, the two lowest E'' bands (210 and 556 cm^{-1}) are assigned as components of ν_6' [$6_0^1(E'')$ and $6_0^2(E'')$, respectively]. The unusual assignment of $6_0^1(E'')$ at 210 cm^{-1} is supported by the presence of a relatively intense sequence hot band $6_1^1(E'')$ at -476 cm^{-1}. From these arguments it is not obvious how the remaining two E'' features below $(0,0) + 1000$ cm^{-1} should be labeled and we defer this discussion until Sec. VI.

Finally, the origin region will be discussed at greater length. An unusual feature appears at -24 cm^{-1}, as shown in Fig. 5, which is not reproduced in rotational contour calculations of the E'' origin. The most obvious assignment is $16_1^1(E')$ but there are a number of observations which tend to contradict this assignment. The -24 cm^{-1} peak does not appear to increase enough in intensity upon heating to 100 °C to be $16_1^1(E')$, but overlap with the origin contour and poor signal to noise ratio at 100 °C make this result inconclusive. Moreover, such

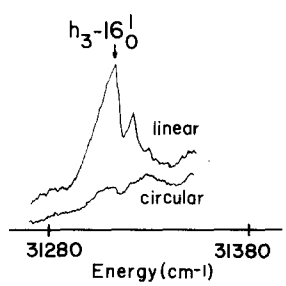

FIG. 9. Experimental rotational contour for h_3-*sym*-triazine $16_0^1(A_1')$ in both linear and circular polarization. The rotationless origin is marked with an arrow. The second polarized peak is a different transition, probably $10_0^1(A_1')$.

a feature is not observed to be associated with other E'' contours (see Figs. 5–8) and one would expect analogous sequence structure to appear on every feature of appropriate symmetry [i.e., $6_0^1\,16_1^1\,(E')$ and $6_0^2\,16_1^1\,(E')$]. It should be noted that $6_0^1\,16_1^1\,(A_1')$ and $6_0^2\,16_1^1\,(A_1')$ are observed. That such a feature is indeed missing on the other E'' contours is confirmed by the fact that a ν_6'' hot band of the -24 cm^{-1} peak is easily observed, whereas no ν_6'' hot bands of the missing $6_0^1\,16_1^1\,(E')$ and $6_0^2\,16_1^1\,(E')$ can be seen. A feature analogous to the -24 cm^{-1} one does appear on the contour of the first totally symmetric one built on the origin $12_0^1\,(E'')$. The ν_6'' hot band built on the -24 cm^{-1} feature is in fact more intense than $6_1^0\,(E'')$, indicating that it might be of the sequence type, namely, $6_1^1\,(A_1'')$. This suggests that the -24 cm^{-1} feature could be related to the presence of $\nu_6'\,(A_1'')$ at the origin. How such a transition could obtain intensity is unclear, but since it is so near an intense feature, many perturbation mechanisms could be envisioned. Further discussion of this feature is postponed until JT calculations are discussed. J. Parkin has communicated to us that the one photon spectrum may also evidence an A_1'' feature "below the E'' origin."

V. CALCULATIONS

A. $(E''+A_2'')\times e'$ vibronic coupling

General methods for vibronic coupling calculations may be found in Refs. 21–23. A brief outline of the calculation is given here. We wish to emphasize that in spite of the differences between MF_6 and triazine, the overall methods and even the results are quite similar.

The two lowest excited states of *sym*-triazine are energetically close (~1500 cm^{-1}); thus, vibronic coupling calculations should include not only vibronic coupling within the E'' manifold, but also between E'' and A_2'' manifolds. The Hamiltonian includes both LJT and QJT terms between E'' components but only linear terms between E'' and A_2'' components.

Since large matrices are diagonalized numerically, it is important to choose a basis set and phase convention

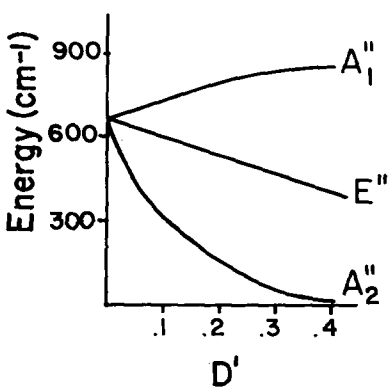

FIG. 10. Effect of LPJT parameter D' on the first quantum of the e' vibration in the $^1E''$ electronic state. $\nu_6'=670$ cm^{-1}. D, $Q[a']$, and $Q[e']$ are zero; ΔE, the separation of the E'' and A_2'' electronic states, is 1500 cm^{-1}. Note that for this case, as well as for the LJT parameter D, the A_2'' level is *below* the E'' level, contrary to observation.

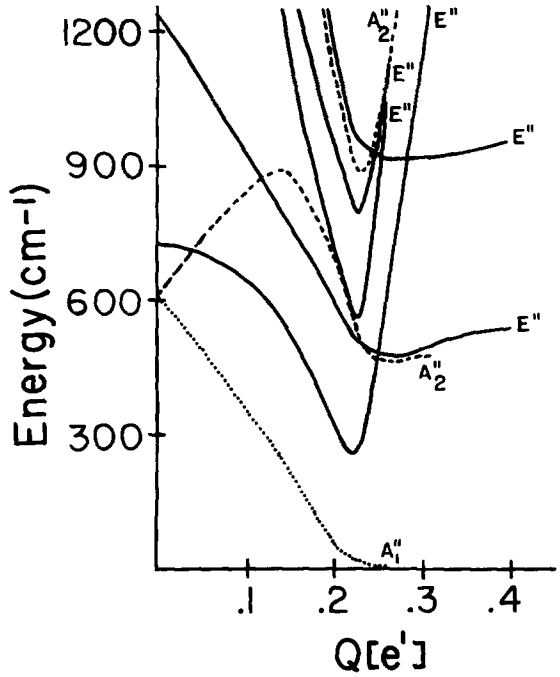

FIG. 11. Effect of QJT parameter $Q[e']$ on ν_6 energy levels in the $^1E''$ state with small LJT parameter $D=0.05$, and $D'=0.0$ $Q[a']=0.0$, $\nu_6'=670$ cm^{-1}. The best fit (see Table VI) was found with $Q[e']=0.2$, but with $\nu_6'=650$ cm^{-1}.

which guarantees real matrix elements. Lax's convention seems most convenient for this purpose.[28] D_{3h} basis functions, matrix representations, and Clebsch–Gordan coefficients are then defined. A vibronic coupling matrix Hamiltonian appropriate for the $(E''+A_2'')$ manifold is formed in the usual fashion utilizing the Wigner–Eckart theorem to reduce the number of independent parameters to the minimum determined by symmetry: D is the LJT parameter; $Q[a_1']$ and $Q[e']$ are the QJT parameters; D' is the LPJT parameter which gauges the vibronic interaction between the E'' and A_2'' manifolds; and ΔE is their separation. Next, a symmetry-adapted vibronic basis is formed. The first step is to determine appropriate combinations of two-dimensional harmonic oscillator functions of the usual polar coordinate type which transform according to the irreducible representations of D_{3h}. These may then be combined with electronic factors using Clebsch–Gordan coefficients. Secular energy matrices are formed by taking matrix elements of the symmetry adapted basis functions with the matrix Hamiltonian. Separate E'', A_2'', and A_1'' blocks are thereby formed. General formulas for the matrix elements of harmonic oscillator function with powers of vibrational coordinates are available.[29] We have used a basis formed from all appropriate harmonic oscillator functions up to $n=20$. Details of this calculation are given in the appendix.

Examples of these calculations are given in Figs. 10 and 11 and Table V. In Fig. 10, the effect of LPJT coupling is illustrated; in Fig. 11 the regime of large QJT coupling with only a small LJT parameter is explored. These calculations will be compared with the experimental findings in Sec. VI. Table V provides precise

TABLE V. Eigenvalue calculation for comparison purposes. (D is the LJT parameter, D' is the LPJT parameter, $Q[a']$ and $Q[e']$ are QJT parameters, ν_6' is the unperturbed frequency, and ΔE is the separation of $^1E''$ and $^1A_2''$.

20 Oscillators				
$D=0.8$	$D'=0.0$	$Q[a']=0.1$	$Q[e']=0.1$	$\nu_6'=670$ cm^{-1}
E''		A_1''		A_2''
0.0		121.0730768		662.5011750
544.2449932		836.4067343		1335.080923
933.4890954		1594.795278		2030.169769
1217.029648		1853.831997		2289.965194
1452.966477		2370.623305		2781.397675
1761.027421		2685.216268		3171.999172
1880.895019		3036.137014		3306.544160
2229.304175		3336.987600		3707.878153
10 Oscillators				
$D=0.1$	$D'=0.1$	$Q[a']=0.1$	$Q[e']=0.1$	$\nu_6'=670$ cm^{-1}
		$\Delta E=2000$ cm^{-1}		
0.0		381.8399697		710.7872126
709.6421346		1263.695364		1437.040730
1006.593879		1719.539355		2038.781471
1388.928001		2133.142081		2288.459417
1613.615720		2480.052105		2317.805388
1871.777141		3013.560704		2791.887116
2115.287101		3137.603136		3080.915056

numerical data which will allow comparison with other calculations.

B. Rotational contour calculations

The rotational contour calculations were carried out in the usual manner.[19,30–32] *Sym*-triazine nuclear statistical weights were employed but seem to make little difference in the contours at the resolution used (0.5 cm^{-1}). The quantum number J was varied from 0 to 100. No line shape function was used for the individual transitions; all intensity was placed in a box covering 0.5 cm^{-1} and the points thus generated were connected with lines on a computer plotter.

VI. JAHN-TELLER INTERPRETATION OF THE ν_6' MODE

The behavior of ν_6 in the E'' electronic state of *sym*-triazine is clearly highly unusual: large energy differences between $6_0^1(A_2'')$ and $6_0^1(E'')$, an anharmonic ν_6 progression, and many E'' modes within a 1000 cm^{-1} of the E'' origin. Reasons for this abnormal behavior are discussed in this section.

The electronic degeneracy of the E'' electronic state and the proximity of an A_2'' electronic (~1500 cm^{-1}) state strongly suggest that some form of vibronic interaction (JT or PJT) is responsible for the highly irregular nature of ν_6' bands.

It is immediately clear upon examining Fig. 10 that PJT interaction between E'' and A_2'' electronic states is not responsible for the observed ν_6' behavior since it places the E'' ν_6 vibronic components *above* the A_2'' ν_6 components. Experimentally, the lowest E'' ν_6' is observed at 210 cm^{-1}, and one photon experiments place the A_2'' (6_0^1) at 677 cm^{-1}. Table VI shows that there is, however, a set of parameters for the JT calculation which qualitatively accounts for the observed ν_6' bands. In fact, the 693 cm^{-1} band which is not assigned in Sec. IV fits well as 6_0^3 (E'') and indeed is predicted to have considerable intensity. Based on these calculations, 6_0^4 is most likely assigned as the 836 cm^{-1} (E'') feature (see Table III for other possibilities, however). Strength of the $n\nu_6$ series interpretation is evidenced by the fact that six energy levels are approximately calculated with only two parameters (see Table VI). [Note that due to the extensive mixing of the $n\nu_6'$ basis set for $n>2$ (see Fig. 11), 6_0^3 (E''), 6_0^4 (E''), etc., should be construed as "the third, fourth, etc.," E'' level of the ν_6' manifold and not necessarily as an E'' arising from a specific single overtone.] The calculation also reproduces the observations that A_2'' levels in the 0–1500 cm^{-1} region above the origin are sparse, and that there are many E'' levels in the 0–1500 cm^{-1} range. Moreover, an A_1'' comes into near coincidence with the origin, in agreement with the perturbed origin contour.

The small Coriolis coupling constant obtained from the rotational contour analysis of the E'' origin (Sec. V B) supports the above interpretation since JT vibronic coupling is expected to quench electronic angular momentum. Further evidence for a substantial JT effect in the ν_6' progression is apparent from the variation of the moments of inertia for triazine in the $n\nu_6'$ vibronic states; these are, respectively, for $n=0$ to 3, 0.2126, 0.2172, 0.2126, and 0.2121.

Calculated intensity patterns for 6_n^1 (A_2'') emission does not agree well with the observed ones as reported in SVLF studies.[14,15] Inspection of the ν_6' (A_2'') 677 cm^{-1} eigenvector calculated with parameters D, D', $Q[e']$, and ν^0 given in Table VI shows $I(6_3^1)$ larger than observed relative to $I(6_2^1)$ and $I(6_4^2)$. The proximity of 6_0^1 (A_2'') at 677 cm^{-1} and 6_0^3 (E'') at 693 cm^{-1} may perturb the observed pattern, however. It is not unreasonable to ex-

TABLE VI. Calculated best fit for ν_6 energy levels in the $^1E''$ state.[a]

$\nu_6'=650$ cm^{-1}		$D=0.05$	$D'=0.0$		$Q[a']=0.0$		$Q[e']=0.2$
	E''		A_1''			A_2''	
Calc.	Obs.	$n=0$ coeff.	Calc.	Obs.	Calc.	Obs.	$n=1$ coeff.
0	0	0.625	46	−24(?)	665	677	0.144
301	227	−0.634	445	···	1060	1176	−0.355
576	556	−0.138	889	···	1369	···	0.750
685	693	−0.348					
917	836(?)	0.055					

[a]Frequencies in cm^{-1}; rotationless spacings are given.

pect only qualitative agreement here since several approximations have been made. Improvements might be realized by including cubic terms or simultaneous JT coupling with other e' vibrational modes (e.g., ν_8').[22] Certainly, extensive Herzberg–Teller couplings are to be expected for this system and have been largely ignored in the calculation.

While substantial JT coupling in the E'' electronic manifold is probably to be expected, it is however counterintuitive that the QJT parameter $Q[e']$ is greater than the LJT parameter D. It may be that there is some "hidden" or approximate symmetry present in *sym*-triazine which tends to minimize LJT coupling. For example, many of the molecular orbitals of *sym*-triazine possess near cylindrical symmetry. Since ν_6' is an in-plane vibration, the entire electronic and vibrational coupling may mimic the cylindrical symmetry of a linear molecule; it is well known that LJT terms are zero for linear molecules (the Renner–Teller effect).

VII. CONCLUSIONS

Two photon photoacoustic spectra of the lowest excited state $^1E''$ of *sym*-triazine have been obtained. The electronic symmetry has been shown to be E'' by direct observation of rotational contours of the origin band and by observation of hot bands associated with this origin. Electronic angular momentum of this state is quenched ($\zeta_e \sim 0.1$). ν_6' vibronic components dominate the remainder of the spectrum from 0–1500 cm^{-1} and possess highly irregular intervals. Large splittings exist between A_1'', A_2'', and E'' vibronic ν_6' components.

It has been possible to fit and explain such an unusual progression for ν_6' based on a vibronic coupling calculation which has QJT coupling terms $Q[e']$ larger by a factor of 4 than LJT coupling terms D. PJT coupling with the nearby A_2'' state appears not to be important for this energy level scheme.

The two photon photoacoustic experimental technique has been demonstrated to be a sensitive method for obtaining the data. It is complementary to fluorescence excitation detection techniques. Through the use of photoacoustic detection, interference of CN photochemiluminescence was eliminated. The CN emission did, however, reproduce the photoacoustic spectrum in all essential features.

Note added: During the refereeing process, it has been pointed out to us by Professor G. J. Small that the crystal spectra of *sym*-triazine evidence weak relatively broad features at (0, 0) + 210 cm^{-1} and (0, 0) + 536 cm^{-1} (see Ref. 8, Fig. 6). We have noted these coincidences [with (0, 0) + 227 cm^{-1} and (0, 0) + 556 cm^{-1}] ourselves but have refrained from commenting on them because of the difference in frequency, the difficulty of making such comparisons in general, and the realization that our arguments are not particularly strengthened by this comparison. Nonetheless, we agree with Professor Small's evaluation that 6_0^1 (E'') and 6_0^2 (E'') may well be crystal induced at (0, 0) + 201 cm^{-1} and (0, 0) + 536 cm^{-1}, respectively.

ACKNOWLEDGMENT

We would like to thank Dr. J. Parkin for giving us a copy of J. Barnard's thesis, and for helpful discussions about *sym*-triazine over the years.

APPENDIX: DESCRIPTION OF $(E''+A_2'')\times e'$ VIBRONIC COUPLING CALCULATION

A vibronic basis made up of electronic ($\psi_{-1}^{E''}$, $\psi_{+1}^{E''}$, $\psi^{A_2''}$) and two-dimensional harmonic oscillator functions ($\chi_{N,L}$) is generated, and symmetry types E'', A_1'', and A_2'' are grouped together. E'' basis functions of the (-1) type were used. For $N=0$ to $N=20$, L was run over its values $N, N-2, \ldots, 1$ or 0. For a given (N, L), basis functions were generated from the following forms:

E''

$L=0$,	$\chi_{N,0}\psi_{-1}^{E''}$,
MOD$(L,3)=0$, MOD$(L,2)=0$, $L\neq 0$,	$\sqrt{\frac{1}{2}}(\chi_{N,L}+\chi_{N,-L})\psi_{-1}^{E''}(E''\times a_1')$, $\sqrt{\frac{1}{2}}(\chi_{N,L}-\chi_{N,-L})\psi_{-1}^{E''}(E''\times a_2')$,
MOD$(L,3)=0$, MOD$(L,2)=1$,	$\sqrt{\frac{1}{2}}\,i(\chi_{N,L}-\chi_{N,-L})\psi_{-1}^{E''}(E''\times a_1')$, $\sqrt{\frac{1}{2}}\,i(\chi_{N,L}+\chi_{N,-L})\psi_{-1}^{E''}(E''\times a_2')$,
MOD$(L,3)=1$, MOD$(L,2)=0$,	$\chi_{N,L}\psi_{+1}^{E''}$, $\chi_{N,-L}\psi^{A_2''}$,
MOD$(L,3)=1$, MOD$(L,2)=1$,	$-i\chi_{N,L}\psi_{+1}^{E''}$, $i\chi_{N,-L}\psi^{A_2''}$,
MOD$(L,3)=2$, MOD$(L,2)=0$,	$\chi_{N,-L}\psi_{+1}^{E''}$, $\chi_{N,L}\psi^{A_2''}$,
MOD$(L,3)=2$, MOD$(L,2)=1$,	$-i\chi_{N,-L}\psi_{+1}^{E''}$, $i\chi_{N,L}\psi^{A_2''}$;

A_1''

MOD$(L,3)=1$, MOD$(L,2)=0$,	$\sqrt{\frac{1}{2}}(\chi_{N,L}\psi_{-1}^{E''}+\chi_{N,-L}\psi_{+1}^{E''})$,
MOD$(L,3)=1$, MOD$(L,2)=1$,	$\sqrt{\frac{1}{2}}\,i(-\chi_{N,L}\psi_{-1}^{E''}+\chi_{N,-L}\psi_{+1}^{E''})$,
MOD$(L,3)=2$, MOD$(L,2)=0$,	$\sqrt{\frac{1}{2}}(\chi_{N,-L}\psi_{-1}^{E''}+\chi_{N,L}\psi_{+1}^{E''})$,
MOD$(L,3)=2$, MOD$(L,2)=1$,	$\sqrt{\frac{1}{2}}\,i(-\chi_{N,-L}\psi_{-1}^{E''}+\chi_{N,L}\psi_{+1}^{E''})$,
MOD$(L,3)=0$, MOD$(L,2)=0$, $L\neq 0$,	$\sqrt{\frac{1}{2}}(\chi_{N,L}-\chi_{N,-L})\psi^{A_2''}$,
MOD$(L,3)=0$, MOD$(L,2)=1$,	$\sqrt{\frac{1}{2}}\,i(\chi_{N,L}+\chi_{N,-L})\psi^{A_2''}$;

A_2''

$\mathrm{MOD}(L,3)=1\ ,\ \mathrm{MOD}(L,2)=0\ ,\quad \sqrt{\tfrac{1}{2}}\,(\chi_{N,L}\psi_{-1}^{E''}-\chi_{N,-L}\psi_{+1}^{E''})\ ,$

$\mathrm{MOD}(L,3)=1\ ,\ \mathrm{MOD}(L,2)=1\ ,\quad -\sqrt{\tfrac{1}{2}}\,i(\chi_{N,L}\psi_{-1}^{E''}+\chi_{N,-L}\psi_{+1}^{E''})\ ,$

$\mathrm{MOD}(L,3)=2\ ,\ \mathrm{MOD}(L,2)=0\ ,\quad \sqrt{\tfrac{1}{2}}\,(\chi_{N,-L}\psi_{-1}^{E''}-\chi_{N,L}\psi_{+1}^{E''})\ ,$

$\mathrm{MOD}(L,3)=2\ ,\ \mathrm{MOD}(L,2)=1\ ,\quad -\sqrt{\tfrac{1}{2}}\,i(\chi_{N,-L}\psi_{-1}^{E''}+\chi_{N,L}\psi_{+1}^{E''})\ ,$

$L=0\ ,\quad \chi_{N,0}\psi^{A_2''}\ ,$

$\mathrm{MOD}(L,3)=0\ ,\ \mathrm{MOD}(L,2)=0\ ,\ L\neq 0\ ,\quad \sqrt{\tfrac{1}{2}}\,(\chi_{N,L}+\chi_{N,-L})\psi^{A_2''}\ ,$

$\mathrm{MOD}(L,3)=0\ ,\ \mathrm{MOD}(L,2)=1\ ,\quad \sqrt{\tfrac{1}{2}}\,i(\chi_{N,L}-\chi_{N,-L})\psi^{A_2''}\ .$

The basis functions can be written in the general form

$$\phi_{N,L}=(a\chi_{N,L}+b\chi_{N,-L})\psi_{-1}^{E''}+(c\chi_{N,L}+d\chi_{N,-L})\psi_{+1}^{E''}+(e\chi_{N,L}+f\chi_{N,-L})\psi^{A_2''}\ .$$

Once the basis is generated, the matrix elements must be calculated. Only the upper (or lower) half of the matrix need be calculated, since the matrix is symmetric.

For linear JT coupling within the E'' state we need the matrix Hamiltonian

$$\mathcal{H}_{\mathrm{LJT}}=\begin{bmatrix}\mathcal{H}_0 & ikQ_- & 0\\ -ikQ_+ & \mathcal{H}_0 & 0\\ 0 & 0 & 0\end{bmatrix}$$

and the primitive matrix elements

$$\langle\chi_{N,L}|Q_\pm|\chi_{N+1,L\mp1}\rangle=[(N\mp L+2)/2\alpha]^{1/2}\ ,\quad \alpha=\omega/\hbar\ .$$

The LJT matrix elements can be worked out to

$$\langle\phi_{N,L}|\mathcal{H}_{\mathrm{LJT}}|\phi_{N+1,L+1}\rangle=i\hbar\omega[(N+L+2)D]^{1/2}(a^*c'-d^*b')\ ,$$

$$\langle\phi_{N,L}|\mathcal{H}_{\mathrm{LJT}}|\phi_{N+1,L-1}\rangle=i\hbar\omega[(N-L+2)D]^{1/2}(b^*d'-c^*a')\ ,$$

in which the primed coefficients are from the ket basis function, and $D=k^2/2\hbar\omega^3$.

Similarly, the quadratic Hamiltonians are

$$\mathcal{H}_{\mathrm{QJT}}^{a'}=\begin{bmatrix}\mathcal{H}_0+\frac{ca}{2}Q_+Q_- & 0 & 0\\ 0 & \mathcal{H}_0+\frac{ca}{2}Q_+Q_- & 0\\ 0 & 0 & 0\end{bmatrix},$$

$$\mathcal{H}_{\mathrm{QJT}}^{e'}=\begin{bmatrix}\mathcal{H}_0 & C_eQ_+^2 & 0\\ C_eQ_-^2 & \mathcal{H}_0 & 0\\ 0 & 0 & 0\end{bmatrix}.$$

The relevant primitive matrix elements are

$$\langle N,L|Q_\mp^2|N,L\pm2\rangle=\frac{1}{2\alpha}[4(N\mp L)(N\pm L+2)]^{1/2}\ ,$$

$$\langle N,L|Q_\mp^2|N+2,L\pm2\rangle=\frac{1}{2\alpha}[(N\pm L+2)(N\pm L+4)]^{1/2}\ ,$$

$$\langle N,L|Q_+Q_-|N,L\rangle=\frac{1}{2\alpha}(2N+2)\ ,$$

$$\langle N,L|Q_+Q_-|N+2,L\rangle=\frac{1}{2\alpha}[(N+L+2)(N-L+2)]^{1/2}\ .$$

The quadratic JT diagonal matrix elements are then ($\langle E''\times a_1''|\mathcal{H}_{\mathrm{QJT}}^{a'}|E''\times a_2''\rangle=0$)

$$\langle\phi_{N,L}|\mathcal{H}_{\mathrm{QJT}}^{a'}|\phi_{N,L}\rangle=\hbar\omega(1+Q[a']/2)(N+1)\ ,\quad Q[a']=\frac{C_a}{\omega^2}\ ,$$

$$\langle\phi_{N,1}|\mathcal{H}_{\mathrm{QJT}}^{e'}|\phi_{N,1}\rangle=2Q[e']\hbar\omega(N+1)(a^*d'+d^*a')\ ,\quad Q[e']=\frac{C_e}{2\omega^2}\ .$$

For diagonal in N and off diagonal in L we have

$$\langle\phi_{N,L}|\mathcal{H}_{\mathrm{QJT}}^{e'}|\phi_{N,L+2}\rangle=2Q[e']\hbar\omega[(N-L)(N+L+2)]^{1/2}(b^*d'+c^*a')\ ,$$

$$\langle\phi_{N,L}|\mathcal{H}_{\mathrm{QJT}}^{e'}|\phi_{N,L-2}\rangle=2Q[e']\hbar\omega[(N+L)(N-L+2)]^{1/2}(a^*c'+d^*b')\ .$$

These two formulas must be corrected for $L=0$ in either the bra or ket, since they do not account for the fact that since $L=-L$, a primitive matrix element that is usually zero is nonzero. For $\langle\phi_{N,0}|\mathcal{H}_{\mathrm{QJT}}^{e'}|\phi_{N,2}\rangle$, $2Q[e']\hbar\omega[N(N+2)]^{1/2}d'$ must be added to the above and for $\langle\phi_{N,2}|\mathcal{H}_{\mathrm{QJT}}^{e'}|\phi_{N,0}\rangle$, $2Q[e']\hbar\omega[N(N+2)]^{1/2}d^*$ must be added to the above. The quadratic matrix elements off diagonal in N and diagonal in L are

$$\langle\phi_{N,L}|\mathcal{H}_{\mathrm{QJT}}^{a'}|\phi_{N+2,L}\rangle=\frac{\hbar\omega}{4}Q[a'][(N+L+2)(N-L+2)]^{1/2}\times(a^*a'+b^*b'+c^*c'+d^*d')\ ,$$

$$\langle\phi_{N,1}|\mathcal{H}_{\mathrm{QJT}}^{e'}|\phi_{N+2,1}\rangle=\hbar\omega Q[e'][(N+1)(N+3)]^{1/2}(a^*d'+d^*a')\ .$$

The quadratic matrix elements off diagonal in N and L are

$$\langle\phi_{N,L}|\mathcal{H}_{\mathrm{QJT}}^{e'}|\phi_{N+2,L+2}\rangle=\hbar\omega Q[e'][(N+L+2)(N+L+4)]^{1/2}(b^*d'+c^*a')\ ,$$

$$\langle\phi_{N,L}|\mathcal{H}_{\mathrm{QJT}}^{e'}|\phi_{N+2,L-2}\rangle=\hbar\omega Q[e'][(N-L+2)(N-L+4)]^{1/2}(a^*c'+d^*b')\ .$$

Again for $L=0$ in the bra or ket we must correct the formulas. For $\langle\phi_{N,0}|\mathcal{H}_{\mathrm{QJT}}^{e'}|\phi_{N+2,2}\rangle$ add $\hbar\omega Q[e'][(N+2)(N+4)]^{1/2}d'$, and for $\langle\phi_{N,2}|\mathcal{H}_{\mathrm{QJT}}^{e'}|\phi_{N+2,0}\rangle$ add $\hbar\omega Q[e'][(N+2)N]^{1/2}d^*$.

The matrix elements up to $n=10$ were also hand cal-

culated, and the hand calculation checked by the upper half of the matrix agreeing with the lower half.

The pseudo-Jahn–Teller interaction between the E'' and A_2'' was completed for basis functions to $N=10$, and the matrix elements were hand calculated. The PJT matrix Hamiltonian is

$$\mathcal{H}_{\mathrm{PJT}}=\begin{bmatrix} 0 & 0 & -ik'Q_+ \\ 0 & 0 & -ik'Q_- \\ ik'Q_- & ik'Q_+ & 0 \end{bmatrix} .$$

We have derived the PJT matrix element formulas. They are as follows, with $D'=(k')^2/2\hbar\omega^3$:

$$\langle\phi_{N,L}|\mathcal{H}_{\mathrm{PJT}}|\phi_{N+1,L+1}\rangle=-i\hbar\omega[(N+L+2)D']^{1/2}(b^*f'+c^*e'),$$

$$\langle\phi_{N,L}|\mathcal{H}_{\mathrm{PJT}}|\phi_{N+1,L-1}\rangle=-i\hbar\omega[(N-L+2)D']^{1/2}(a^*e'+d^*f'),$$

$$\langle\phi_{N,L}|\mathcal{H}_{\mathrm{PJT}}|\phi_{N-1,L+1}\rangle=-i\hbar\omega[(N-L)D']^{1/2}(b^*f'+c^*e'),$$

$$\langle\phi_{N,L}|\mathcal{H}_{\mathrm{PJT}}|\phi_{N-1,L-1}\rangle=-i\hbar\omega[(N+L)D']^{1/2}(a^*e'+d^*f') .$$

We have the following additional factors:

for $\langle\phi_{N,0}|\mathcal{H}_{\mathrm{PJT}}|\phi_{N+1,1}\rangle$, add $-i\hbar\omega[(N+2)D']^{1/2}f'$;

for $\langle\phi_{N,1}|\mathcal{H}_{\mathrm{PJT}}|\phi_{N+1,0}\rangle$, add $-i\hbar\omega[(N+1)D']^{1/2}d^*$;

for $\langle\phi_{N,0}|\mathcal{H}_{\mathrm{PJT}}|\phi_{N-1,1}\rangle$, add $-i\hbar\omega(ND')^{1/2}f'$;

for $\langle\phi_{N,1}|\mathcal{H}_{\mathrm{PJT}}|\phi_{N-1,0}\rangle$, add $-i\hbar\omega[(N+1)D']^{1/2}d^*$.

[1]C. Grundmann and A. Kreutzberger, J. Am. Chem. Soc. 76, 632 (1954).
[2]R. C. Hirt, F. Halverson, and R. G. Schmitt, J. Chem. Phys. 22, 1148 (1954).
[3]J. E. Lancaster and N. B. Colthup, J. Chem. Phys. 22, 1149 (1954).
[4]J. S. Brinen and L. Goodman, J. Chem. Phys. 31, 482 (1959); 35, 1219 (1961).
[5]J. E. Lancaster, R. F. Stamm, and N. B. Colthup, Spectrochem. Acta 17, 155 (1961).
[6]K. K. Innes, J. P. Byrne, and I. G. Ross, J. Mol. Spectrosc. 22, 125 (1967).
[7]Y. Udagawa, M. Ito, and S. Nagakura, J. Mol. Spectrosc. 39, 400 (1971).
[8]G. Fischer and G. J. Small, J. Chem. Phys. 56, 5934 (1972).
[9]R. M. Hochstrasser and A. H. Zewail, Chem. Phys. Lett. 11, 157 (1971); J. Chem. Phys. 55, 5291 (1971).
[10]R. M. Hochstrasser, Chem. Phys. Lett. 17, 1 (1972).
[11]R. M. Hochstrasser, T. S. Lin, and A. H. Zewail, J. Chem. Phys. 56, 637 (1972).
[12]T. J. Aartsma and D. A. Wiersma, Chem. Phys. 1, 211 (1973).
[13]E. R. Bernstein and R. E. Smalley, J. Chem. Phys. 58, 2197 (1973); Chem. Phys. 2, 321 (1973).
[14]A. E. W. Knight and C. S. Parmenter, Chem. Phys. 43, 257 (1979).
[15]A. E. W. Knight and C. S. Parmenter, Chem. Phys. 15, 85 (1976).
[16]P. R. Nott and B. K. Selinger, Aust. J. Chem. 31, 1889 (1978).
[17]J. D. Webb, K. M. Swift, and E. R. Bernstein, J. Mol. Struct. 61, 285 (1980).
[18]J. H. Callomon, T. M. Dunn, and I. M. Mills, Philos. Trans. R. Soc. London Ser. A 259, 499 (1965).
[19]F. Metz, W. E. Howard, L. Wunsch, H. J. Neusser, and E. W. Schlag, Proc. R. Soc. (London) A 363, 381 (1978).
[20]J. van Egmond and J. H. van der Waals, Mol. Phys. 28, 457 (1974).
[21]G. R. Meredith, J. D. Webb, and E. R. Bernstein, Mol. Phys. 34, 995 (1977).
[22]E. R. Bernstein and J. D. Webb, Mol. Phys. 37, 191 (1979).
[23]E. R. Bernstein and J. D. Webb, Mol. Phys. 36, 1113 (1978).
[24]J. Barnard, Ph. D. thesis, University College, London (1974).
[25]R. E. Smalley, Ph. D. thesis, Princeton University (1973).
[26]J. J. Barrett (private communication).
[27]K. M. Chen and E. S. Yeung, J. Chem. Phys. 69, 43 (1978).
[28]M. Lax, *Symmetry Principles in Solid State and Molecular Physics* (Wiley-Interscience, New York, 1974).
[29]C. DiLauro, J. Mol. Spectrosc. 41, 598 (1972).
[30]W. Martin McClain and Robert A. Harris, *Excited States*, edited by E. C. Lim (Academic, New York, 1977), Vol. 3, p. 1–56.
[31]L. Wunsch, F. Metz, H. J. Nuesser, and E. W. Schlag, J. Chem. Phys. 66, 386 (1977).
[32]J. R. Lombardi, R. Wallenstein, T. W. Hänsch, and D. M. Friedrich, J. Chem. Phys. 65, 2357 (1976).